Heliyon 8 (2022) e10004

Contents lists available at ScienceDirect

Heliyon

journal homepage: www.cell.com/heliyon

Research article

Attenuation of nitrate from aqueous solution using raw and surface modified biosorbents from *Adansonia digitata* fruit pericarp

David Mihayo, Maheswara Rao Vegi *, Said Ali Hamad Vuai

The Department of Chemistry, College of Natural and Mathematical Sciences, The University of Dodoma, Dodoma, P. O. Box: 259, Tanzania

ARTICLE INFO

Keywords:
Biosorption
Nitrate
Response surface methodology (RSM)
Adsorption isotherms
Adsorption kinetics

ABSTRACT

The prevalence of nitrate in potable water is a serious environmental concern. Several methods for eliminating nitrate from water have been made and implemented. During the course of this research, raw (RADFP) and surface-modified fruit pericarp (SMADFP) biosorbents derived from the *Adansonia digitata* plant were applied in order to remove nitrate from an aqueous solution. The external features of the biosorbents were studied with the aids of SEM and BET. The FT-IR spectrometer was utilized for identification of the functional groups of the adsorbents. A UV-Vis device was used to quantify the nitrate concentration. The adsorbents under investigation exhibit a heterogeneous pore structure with a considerable number of mesopores, with surface areas of 361.527 and 379.877 m^2 per gram for RADFP and SMADFP, respectively. FT-IR spectra revealed the presence of carboxyl, hydroxyl, carbonyl, and halogen groups on the adsorbent. The maximum nitrate removal efficiencies of RADFP and SMADFP were 64.55 and 88.95%, respectively. The maximum adsorption efficiencies are achieved when the pH is 2, the starting concentration is 27.50 mg/L, the contact period is 75.00 min, and the amount of biosorbent is 5.50 g. RADFP and SMADFP have a removal capacity of 12.45 as well as 25.18 mg per gram and adsorption intensity of 3.2300 and 5.4500, respectively. The investigational values for the elimination of nitrate ions concurred well to both Freundlich and Langmuir models with R^2 values of 0.99917 and 0.99763 for RADFP and SMADFP, respectively, and pseudo-second-order kinetic model with R^2 values of 0.99817 and 0.99947, respectively for RADFP and SMADFP. It can be concluded that SMADFP is a relatively better biosorbent than RADFP, which will be utilizable for the remediation of nitrate from an aqueous solution.

1. Introduction

Water scarcity is a big issue in every country. Freshwater constitutes three percent of the total water supply available for home use globally. The majority of this freshwater is found as groundwater in frozen soil moisture and deep underground aquifers, with lakes and rivers accounting for less than 1% of total freshwater (Mohsenipour et al., 2014). However, rain and snowfall replenish it regularly, making it available on a long-term basis (Al-Fatlawi and Neamah 2015). Drinkable water is essential for humans and other living species. However, a range of pollutants, including nitrate ions, deteriorate the consistency of water utilized by animals and humans (Grassi et al., 2012).

Human activities are the most common source of water pollution, but there are also natural sources, such as silt and sediments eroded by nature, natural oil seeps, and organic materials swept into streams by strong rains and flooding (Ideriah et al., 2013). Free nitrogen pollution in drinking water is frequently created by microorganisms in the soil, water, and garbage that convert it to nitrite and nitrate, as well as turn nitrate back to nitrite. Among the anthropogenic sources are new farming methods that employ chemicals, animal waste runoff from dairies and feedlots, and seepage of human sewage from private septic tanks, all of which have found their way into the water supply and plant tissues (Kihampa and Mwegoha 2010; Kihampa 2013). However, nitrogen-enriched agricultural fertilizers are the primary cause of nitrate contamination in the environment (Mohsenipour et al., 2014).

Nitrate is a chemical substance that is considered non-toxic. In the saliva and gastrointestinal system, approximately 5% of all consumed nitrate is converted to the more poisonous nitrite, which is harmful to the body. Chronic hazardous effects of nitrate are only generated by the nitrite formed during bacterial enzymatic reduction, which is the only source of these effects. As shown in Eq. (1) (Soumya et al., 2015), nitrite has the ability to react with haemoglobin (oxyHb), which results in the formation of methemoglobin (metHb) and nitrate.

* Corresponding author.
E-mail address: vegimahesh@gmail.com (M.R. Vegi).

https://doi.org/10.1016/j.heliyon.2022.e10004
Received 10 October 2021; Received in revised form 20 February 2022; Accepted 14 July 2022

$$NO_2^- + \text{oxyHb}(Fe^{2+}) \rightarrow \text{metHb}(Fe^{3+}) + NO_3^- \quad (1)$$

Nitrite degrades haemoglobin in the bloodstream, converting it to methemoglobin. This dysfunctional form is incapable of transporting oxygen thus reducing blood oxygenation and potentially inducing tissue hypoxemia. As a consequence, the body's cells are deprived of the oxygen they need to function properly, which is referred to as methemoglobinemia. Due to the fact that the lack of oxygen causes the baby's skin to turn bluish, particularly around the eyes and mouth, this condition is also referred to as the Blue Baby Syndrome in infants. If treatment is not provided, newborns will succumb to this condition and perish Ogata et al., (2018) It is believed that once nitrate is converted to nitrite in the body, it can react with certain foods that contain amines to produce nitrosamines. Nitrosamines are well-known to be powerful substances that cause cancer. A link between stomach cancer and nitrate levels in drinking water has been demonstrated in a few epidemiological studies conducted on human populations. However, numerous studies have established no link between nitrate in drinking water and cancer (Soumya et al., 2015).

To minimize health risks, WHO (2011) and the US EPA established recommended nitrate concentration of 50 and 10 mg/L, respectively, in potable water (Dehghani et al., 2015). However, it has been established that the maximum nitrate concentration that is allowed to be present in drinking water has been exceeded in a great number of countries all over the world (Namasivayam and Holl 2005). As a result, lowering the nitrate level in potable water to safe levels has become a major concern (Elisante and Muzuka 2017).

Because of this, there is need of ways that are both simple and efficient in order to get rid of the excessive nitrate in the water. Numerous techniques for reducing nitrate levels in water have been developed in conjuction with adsorption (Hu et al., 2015). While preventative measures to eliminate nitrate ions have been implemented, each of these approaches has inherent advantages and disadvantages. However, among these approaches, adsorption has shown a significant ability to eliminate contaminants. The adsorption of nitrate ions has been investigated using readily available biowastes (Dubey et al., 2009).

Various locally and non-locally available sourced materials have been proposed and evaluated as adsorbents for nitrate removal research in recent years. Some of the adsorbents used by different researchers include modified natural zeolite (Masukume et al., 2010), rice chaff (Dehghani et al., 2015), chitin (Morghi et al., 2015), banana peel (Reddy et al., 2015), cross-linked, quaternized Chinese reed (Namasivayam and Höll 2005), green algal powder (Sumiya and Anu, 2016). They've proved that they can remove a lot of nitrates. Because these materials are readily available, this approach for removing nitrate from drinking water is inexpensive and efficient.

The challenge now is to identify biosorbents that can eliminate nitrate ions concentrations to safe levels. There has been no article in the literature to date on the use of Baobab (*Adansonia digitata*) fruit pericarp for nitrate attenuation. In Tanzania, the Baobab (*Adansonia digitata*) tree is referred to as 'mbuyu' and is available plenty. It is a member of the Bombaceae family (Tarachand and Dipak 2016). Baobab trees are distributed in many regions of Tanzania in Dodoma, Singida, Tabora, Shinyanga, Simiyu, Arusha, and Manyara. In the year 2016/2017, Tanzania exported 29, 864 kg of baobab products (NBS, 2017). This implies that there is a reasonable amount of baobab waste produced annually. However, no literature shows the statistics of baobab waste produced annually. Baobab trees are also found plenty in South Africa, Botswana, Namibia, Zimbabwe, Benin, Mali, Malawi, Ghana, Kenya, Ethiopia, and other African countries. For instance, the baobab density in Benin ranges from one to five trees per square kilometre (Assogbadjo et al., 2021). The baobab fruit is used by the majority of people as medicine for the treatment of gastrointestinal-related diseases. This is also widely used as food, and beverages (Tukur and Rabi' u, 2013). But, the pericarp is considered an agricultural waste, which leads to pollution in the environment. The main aim of this study is to prepare new biosorbents from the precursor (*Adansonia digitata* fruit pericarp) that is easily available and can be accessed by anybody as it is free from food competition; can be processed and operated easily. The study also characterized the developed biosorbents, optimized different parameters, investigated the adsorption mechanism through adsorption isotherms and kinetic studies, and applied the biosorbents in real water samples. The procedure of preparing the adsorbents does not need qualified personnel and professional engineers. Additionally, utilizing batch adsorption studies and UV-Vis spectrophotometry for nitrate measurement, the nitrate ions in an aqueous solution were treated with produced *Adansonia digitata* fruit pericarp (ADFP) in both raw (RADFP) and surface-modified (SMADFP) forms.

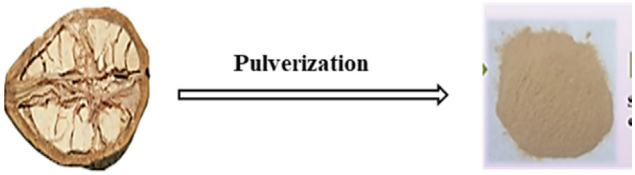

Figure 1. Graphic diagram of raw adsorbent preparation **a** raw *Adansonia digitata* fruit and **b** Powdered *Adansonia digitata* fruit pericarp.

2. Materials and methods

2.1. Materials

Adansonia digitata's pericarp was harvested in Dodoma, Tanzania, and used to create raw and surface-modified adsorbents. All reagents were purchased from RANKEM, India PVT Limited, and were of analytical grade. The following chemicals were used in this study: Sulphuric acid, ethylenediamine, sodamide, sodium hydroxide, hydrochloric acid, iodine, propanol, potassium iodide and manganese (IV) oxide. In order to create the simulated water, 1.37 g of $NaNO_3$ were dissolved in distilled water at a concentration of 1000 mg/L.

2.2. Sample collection of real water

At Nkuhungu village, in the Dodoma region, Tanzania, water samples were taken from three distinct groundwater wells. This was done at a depth of 50 cm to avoid dust and oily substances floating above the wells and collected in the container. To collect groundwater from the three distinct wells, a water sampler HDPE bottle with a 1 L capacity was employed. For sampling reasons, all sampling containers were rinsed with detergents before use and cleaned with deionized water. The containers were cleaned three times with groundwater before being utilized to collect the samples during the test period. Finally, for the digestion procedure, the freshly collected water samples from each well were combined and taken as composite samples. The samples were stored in an icebox and sent to the laboratory for analysis. Because water samples can change over time due to physical, chemical, and biological variables, they were filtered through Whatman filter paper No 41 as soon as they arrived at the Chemistry lab to remove suspended organic matter and microbes. Then kept for the application of biosorbent for the remediation of nitrate.

2.3. Preparation of adsorbents

Both unmodified (raw) and surface-modified adsorbents were prepared in the manner described in detail by Mihayo et al. (2021).

2.4. Preparation of raw adsorbent

Impurities associated with the materials were cleared using distilled water. The pericarp of the baobab was dried in the sun to remove moisture before being heated at 80 °C to a consistent mass. A particle size of approximately 0.250 mm was obtained by crushing and sieving the dried pericarp. The product (Figure 1) was kept in an air-tight container to prevent it from any reactions before characterization and application for nitrate removal (Ali et al., 2012).

2.5. Preparation of surface-modified adsorbent

There were three stages involved in the surface modification. Under ultraviolet light, propanol and chlorine were combined to make dichloropropanol in the first step of the process. At this point, one mole of manganese (IV) oxide was dissolved in an excessive amount of hydrochloric acid to form chlorine gas (5 M). Eq. (2) is a representation of the suggested reaction.

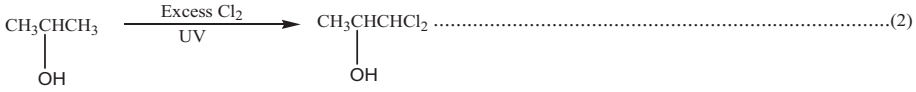

After the first step, the dichloropropanol was deprotonated using $NaNH_2$ as the base. This led to the formation of an alkoxide as well as an epoxide in the second step (in 2:2 volume ratios). The base $NaNH_2$ deprotonates the alcohol, producing an intermediate called an alkoxide that boosts the compound's nucleophilicity. When the alkoxide nucleophile approaches the electrophile C, an SN_2 reaction will take place, which will result in the displacement of the leaving group, which is the halide ion. In order to generate an epoxide, the nucleophile needs to attack the antibond between C and X (Bakar et al., 2016). The proposed reaction is given by Eq. (3)

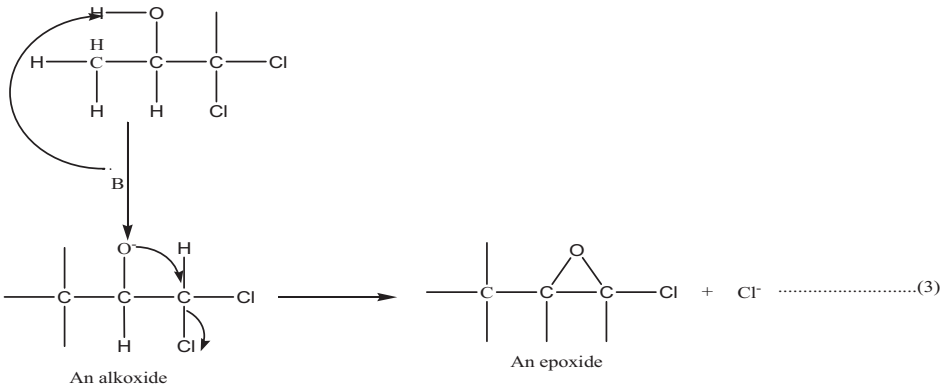

Note: B^- is $NaNH_2$

In the third stage, an epoxide that was produced in the second step was applied to 50 g of powdered pericarp (PP) in dil HCl (0.1 M). In order to create positively charged functional groups, 200 mL of ethylenediamine was added next. Equations (4) and (5) outline the proposed reactions.

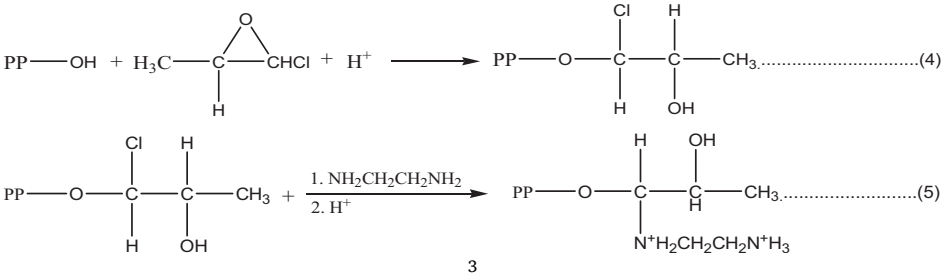

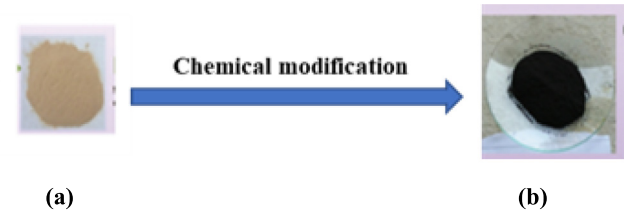

Figure 2. Graphic diagram of SMADFP Preparation **a** Powdered *Adansonia digitata* fruit pericarp **b** SMADFP.

The product obtained (Figure 2) was dried in an oven for 24 h at 100 °C. After that, they underwent a second round of drying in an oven for another 24 h at a temperature of 150 °C, and once they had cooled, they were placed in an airtight container for storage (Rangari and Chavan, 2017).

2.6. Analysis of the properties of adsorbents

2.6.1. Moisture content

The sample with a weight of 5 g was put into a petri plate. It was then heated to 105 °C for 2 h. After heating, it was cooled in a desiccator. The ultimate weight of the dried sample was calculated now. Ali and his coworkers (Ali et al., 2012) discussed how they calculated the moisture content percentage using Eq. (6).

$$\%\ \text{Moisture content} = \frac{\text{Mass of moisture}}{\text{Mass of original sample}} \times 100 \qquad (6)$$

2.6.2. Volatile matter content

The sample's original mass (5 g) was measured and placed in a crucible that was sealed and heated for 7 min at 925 °C in a furnace. After placing the crucible in a desiccator to speed up the cooling process, the ultimate weight of the combusted material was determined. Using Rangari and Chavan's Eq. (7) (2017), the percentage of volatile matter content was determined.

$$\%\ \text{Volatile matter content} = \frac{\text{Weight of volatile matter}}{\text{Weight of original sample}} \times 100 \quad (7)$$

2.6.3. Pore volume and porosity

After putting a known quantity of material (1 g) into a measuring cylinder with a capacity of 10 mL, the volume of the particles was determined. This sample was heated for 5 min in a beaker containing 20 mL of distilled water in order to remove any traces of air that may have been present. Following a period of drying at room temperature for 48 h, the contents were weighed. A calculation was made to determine the sample's pore volume by multiplying the sample's weight by the density of water. To determine the degree of porosity possessed by a particle, its pore volume was divided by its total volume (Gumus and Okpeku 2015).

2.6.4. BET analysis

For the purpose of determining the surface area and pore size of the biosorbents, experiments were performed at a temperature of 77.35 °C using an automated gas sorption analyzer called a Quanta Chrome Nova Win version 11.03. For the purpose of calculating the surface area, the Brunaeur-Emmet-Teller (BET) method was applied.

2.6.5. Iodine number

A normal iodine solution was prepared by dissolving I_2 (2.7 g) and KI (4.1 g) in 1-liter deionized water and storing it in a light-resistant bottle. Under laboratory conditions, a typical iodine solution was treated with activated carbon of three different masses of 1, 3, and 5 g. Filtration was used to isolate the carbon-treated solutions from the treated iodine solution. A standardized solution of 0.1 N sodium thiosulfate was employed in a titration with starch as the indicator in order to determine the amount of iodine that was present in the filtrate. The amount of sodium thiosulphate that was used was noted. Every dose of activated carbon's iodine yield was measured, and the mean results were recorded (Das et al., 2015).

2.6.6. Methylene blue number

10.0 g of activated carbon was mixed with 10.0 mL of methylene blue solution at various concentrations (10, 25, 50, 100, 250, 500, and 1000 mg/L) for 24 h at room temperature. A UV/Visible spectrophotometer was used to determine the remaining methylene blue concentration. The amount of methylene blue adsorbed from each solution was calculated using Eq. (8):

$$q_{eq}\left(\frac{mg}{g}\right) = \frac{C_o - C_e}{M} \times V \quad (8)$$

Where C_0 (mg/L) represents the initial concentration of the methylene blue solution at time equal to zero, C_e (mg/L) represents the concentration of the methylene blue solution at the time of equilibrium, V (L) represents the volume of the solution that was treated, and M (g) represents the mass of the adsorbent (Das et al., 2015).

2.6.7. Morphology

A scanning electron microscope (SEM) (model SSX-550; manufacturing company: Shimadzu, Japan) was used to examine the morphology, pore size, surface area, and volume of RADFP and SMADFP. Scanning electron microscopy (SEM), which uses pictures created by scanning with an electron beam, allows one to see the surface characteristics of solid materials (Tan et al., 2015). Prior to the SEM scanning, the sample was given a coating of gold or silver for 30 s at a current of 50 mA in order to make it conductive (at an accelerating voltage of 15 kV). After that, it was kept into a container for SEM analysis. Magnifications ranging from 20X to 5000X were used to capture scanning electron micrographs of the JSM 6380A.

2.6.8. Anion-exchange capacity

Boehm's titration was expended in this analysis to assess the sorbents' potential for cation and anion exchange (Zhu et al., 2009). After adding 1 g of adsorbent to an Erlenmeyer flask that contained 20 mL of 0.1 M NaOH solution, the flask was shaken. The suspension was shaken for 24 h at a rate of 200 rpm at room temperature (27 ± 2 °C) in order to achieve equilibrium. In order to determine the amount of remaining NaOH in the solution after filtering, a titration was performed using 0.1 M HCl with the aid of phenopthalein indicator.

A calculation was made to determine the amount of NaOH that was adsorbed. The amount of NaOH that was adsorbed onto the surface of the adsorbent was utilised in the calculation of the anion exchange capacity.

2.6.9. pH at the point of zero charge (pH_{pzc})

The usage of the solid addition procedure was used to confirm this. Each of the six 100 mL Erlenmeyer flasks that contained 100 mL of 0.1 M potassium nitrate solution was sealed with 1.0 g of activated carbon. It just took a few drops of solutions containing 0.1 M HCl/NaOH to bring the pH of six different solutions up to 2, 4, 6, 8, 10, and 12. An electrical shaker (25 ± 1 °C) was used to equilibrate the solution mixes at a rate of 200 rpm for 24 h. After that, the suspension of each sample was filtered, and the final pH was calculated. The graph between the original pH and pH curve was used to calculate the value of pH_{pzc} (Tan et al., 2008).

2.6.10. Functional group analysis

According to Das et al. (2015), a Fourier Transform Infrared (FT-IR) Spectrophotometer was utilised in order to identify the bonding patterns of the raw and surface modified adsorbents, as well as the functional groups that were present in the samples. A PerkinElmer spectrum 100 FT-IR spectrometer from the United Kingdom was used to gather the spectra and distinctive peaks. This instrument measured wavenumbers that ranged from 350 to 4000 cm^{-1} and performed 100 scans on each sample with a resolution of 4 cm^{-1}. In order to mill the materials, KCl was utilised (mass ratio of 1:100 for carbon: KCl).

2.6.11. Calibration of the instrument

UV-Visible spectrophotometer was calibrated to ensure the instrument's proper operation and for calculation of contaminant levels. The device was calibrated using five standards of nitrate solutions diluted from a stock solution in the range of 1 mg/L to 50 mg/L before applying each adsorbent. The correlation coefficients (R^2) that were produced by the graphs fall in the range of 0.99956–0.99992. Following calibration, the samples were analyzed for nitrate using a UV-Visible spectrophotometer at a λ_{max} of 410 nm. The removal efficiencies were calculated by comparing the absorbance measurements to the calibration graph.

2.6.12. Quantification of nitrate ions

After adding 5 mL of concentrated HCl and 2 mL of a Zn/NaCl granular mixture to 10 mL of nitrate stock solution (50 mg/L) and allowing the mixture to stand for 30 min with occasional stirring to form nitrite, the solution was filtered into a 100 mL standard flask using Whatman No. 41 filter paper and then diluted to the mark. In a series of 10 mL standard flasks, aliquots of a stock solution containing 5, 15, 25, 35, 45, and 55 mg/L of reduced nitrate were transferred. In order for the diazotization reaction to be finished, 1 mL of sulfanilic acid with a concentration of 0.5% and 1 mL of a solution of 2 M HCl acid were added. The mixture was then vigorously agitated for 5 min. After that, 1 mL of 0.5% methyl anthranilate and 2 mL of 2 M of a solution of sodium hydroxide were added to create an azo dye, and the mixture was diluted with distilled water to a volume of 10 mL. Following the dilution of the

Table 1. Physical characteristics of the adsorbents.

Adsorbents	MC (%) (SD, n = 3)	VM (%) (SD, n = 3)	PV (%) (SD, n = 3)	Porosity (SD, n = 3)	IN (mg/g) (SD, n = 3)	MBN (mg/g) (SD, n = 3)
RAD-FP	13.2 (1.4)	45.1 (2.1)	1.8 (0.6)	0.15 (0.04)	150 (5.5)	120 (3.6)
SMA-DFP	3.7 (0.8)	15.2 (1.2)	2.5 (0.6)	0.28 (0.05)	405 (8.4)	243 (6.3)

MC = Moisture Content, VM = Volatile Matter, PV = Pore Volume, IN = Iodine Number and MBN = Methylene Blue Number, SD = standard deviation, n = number of replicates.

red-colored dye to a volume of 10 mL with water, an absorbance reading at 410 nm was taken using a UV-Vis spectrophotometer and compared to the blank reading for the corresponding reagent. Following calibration, the same technique was used to calculate the concentration of nitrate residue in the synthetic solution using the calibration graph generated by plotting the concentrations of the standard solutions against their corresponding absorbance readings (Dehghani et al., 2015).

2.6.13. Establishment of optimal conditions

The RSM was utilized, a strong statistical technique for optimizing several parameters, to produce sequences of planned experimentations in order to acquire an ideal response (Naik and Setty 2013). All of the following were taken into consideration: the starting concentration, the amount of dose, the interaction period, and the pH. The statistical program Design Expert was used to create the experimental design. Simulation and analysis of the effect of operating parameters on adsorption performance were carried out with the help of the Central Composite Design (CCD). It cuts down on the number of experimental trials that need to be conducted in order to analyse multiple parameters and the interactions between them (Naik and Setty 2013). pH, starting concentration, interaction time, and amount of adsorbent ranged from 2 to 12, 5–50 mg/L, 30–120 min, and 1–10 g, respectively. The Design Expert statistical program was used to calculate the series of experiments and list of parameters to address using these levels.

The adsorbents RADFP and SMADFP were combined with 100 mL of simulated water and physically shaken at 200 rpm at room temperature in order to conduct batch experiments in accordance with the software's experimental settings. The mixture was then filtered using a Whatman No. 42 filter paper. A UV-Visible spectrophotometer was used to determine nitrate concentrations spectrophotometrically. The difference between the solution's initial concentration and the solution's concentration after sorption was used to calculate the levels of the nitrate ion eliminated by the adsorbent. In order to calculate the adsorption capacity and efficiency, respectively, Eqs. (9) and (10) were utilised.

$$\text{Adsorption efficiency} = \frac{[C_o - C_t]}{[C_o]} \times 100 \quad (9)$$

$$\text{Adsorption capacity} = \frac{[C_o - C_t]}{m} \times V \quad (10)$$

Where C_o is the nitrate level before adsorption, C_t is the remainder nitrate level at time t, m is the mass of the adsorbent and V is the volume of the solution used in the batch (100 mL).

2.6.14. Adsorption isotherms

The Langmuir and Freundlich adsorption isotherms were examined at a pH of 6.90 ± 0.10 by increasing the adsorbent dosage from 2 to 10 g and mixing with a 50 mL solution of nitrate (50 mg/L) for 24 h to reach equilibrium at ambient temperature (27 ± 2 °C). The results of the experiments were utilized to calculate all of the values that were necessary to plot the isotherms, as is demonstrated elsewhere (Berhe et al., 2015).

2.6.15. Studies of kinetics

Kinetic experiments were conducted at various time intervals (10–50 min) with the pH adjusted to 6.90 ± 0.10 and the temperature set to room temperature (27 ± 2 °C). Each of these tests began with a volume of 50 mL of a solution containing 50 mg/L of nitrate. The impacts of kinetics experiments were examined using pseudo-first- and second-order models, as outlined by Fan et al. (2003).

2.6.16. Application of adsorbents on the real water

The collected real water samples from groundwater sources were subjected to an adsorption process using batch experiments. The concentrations of nitrate before and after adsorption were determined as explained in the section on quantification of nitrate ions. The initial concentrations of three groundwater samples were 55.4, 56.9, and 62.5 mg/L. The adsorbents were applied to this water in a similar way to that of synthetic water. The adsorption process was carried out at optimized conditions of pH 2, interaction time of 75 min, and amount of adsorbent of 5.50 g.

3. Results and discussion

3.1. Characterization of adsorbents

3.1.1. Moisture content

RADFP and SMADFP had moisture contents of 13.2 and 3.7%, respectively (Table 1). The performance of sorbents that include a smaller amount of moisture is superior to that of sorbents that contain a higher amount of moisture. This is attributed by 3 factors. The first factor is a trace quantity of moisture from the surrounding environment, which wets the surface of the adsorbent and occupies some of the adsorptive space. Second, there is the possibility of competition between nitrate and moisture for the active sites on the adsorbent. Thirdly, the presence of moisture inhibits the entry of nitrate ions into the pore channels (Zhang et al., 2018). As a result, SMADFP exhibits superior adsorption properties in terms of moisture content. The optimal level of moisture content, according to Gumus and Okpeku (2015), is in the range of 3–6%. SMADFP indicated a moisture content within the recommended range.

3.1.2. Volatile matter content

There is a correlation between the presence of volatile organic compounds in the raw materials and the availability of volatile matter. This information reveals whether or not the precursor is suitable for biosorbent synthesis. Both RADFP and SMADFP had volatile matter content, but RADFP's was higher, at 45.1%, than SMADFP's, at 15.2%. Devi et al. (2012) recorded volatile matter contents between 20.67 and 22.67% for the activated carbon prepared from coconut shells. This implies that in the present study, SMADFP is a more effective adsorbent. This indicates that the pericarp of *Adansonia digitata* is ideal for preparing biosorbents.

3.1.3. Pore volume and porosity

RADFP and SMADFP have pore volumes of 1.8 and 2.5 cm^3/g, respectively. Pore volumes of 2–5 cm^3/g were recommended. These data are equivalent to the recommended values and those obtained by Ali et al. (2012) for a bio-sorbent prepared from agricultural wastes (pore volumes of 2.0 and 2.9 cm^3/g). The pore volumes range from medium (mesoporous) to very small (microporous), suggesting that the adsorbents are capable of removing both relatively large and relatively tiny compounds from aqueous solutions.

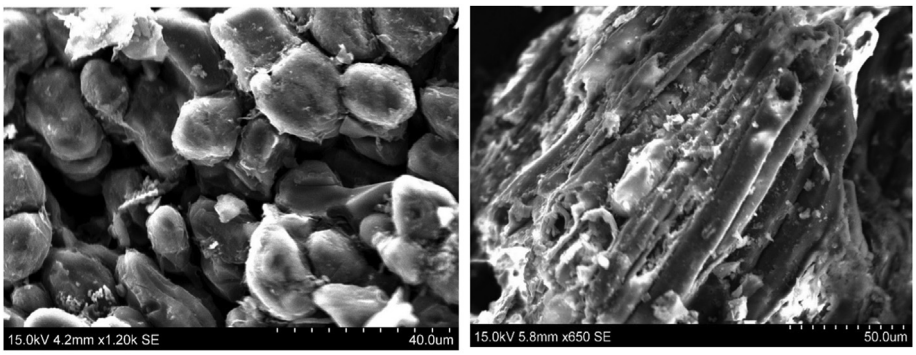

Figure 3. a SEM image of RADFP and **b** SEM image of SMADFP (at a magnification of 15 kV).

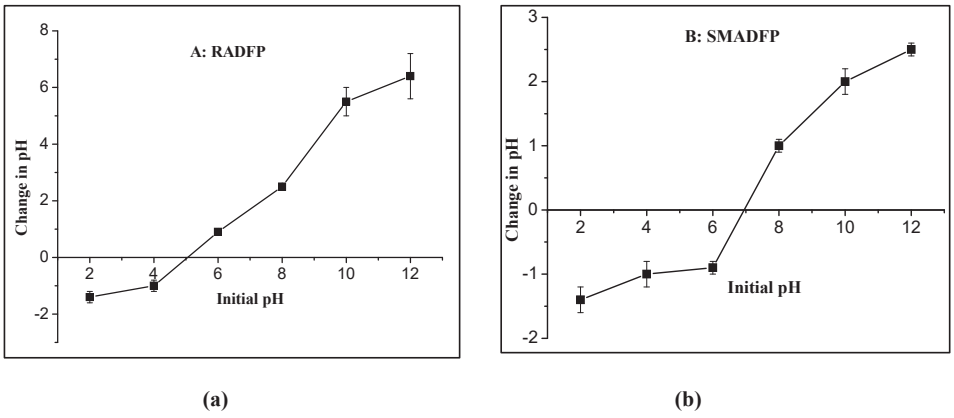

Figure 4. pH at point of zero charge for the adsorbents **a** RADFP **b** SMADFP.

A material's porosity can be defined as the ratio of the volume of its pores to the volume of its overall bulk (adsorbent). Thus, porosity increases the adsorbent's ability for adsorption (Verla et al., 2012). RADFP and SMADFP have a porosity of 0.15 and 0.28, respectively. These values are comparable to those recorded by Gumus and Okpeku (2015) for activated carbon prepared from snail shell wastes (0.28 and 0.38).

3.1.4. BET analysis

RADFP and SMADFP had surface areas of 361.527 and 379.877 m^2/g, respectively. These biosorbents possessed a considerable surface area, implying a high capability for pollutant removal. A considerable number of active sites are contained inside adsorbents that have a surface area in the range of 200–300 m^2/g, some of which contain functional groups, that enhance the adsorption of a wide range of anions and cations from water (Jadhav et al., 2015). RADFP and SMADFP had pore diameters of 0.3032 and 0.3053 nm, respectively. Microporosity is described by the IUPAC as pores with a diameter of less than 2 nm (Ali et al., 2012). The pore diameter revealed the adsorbents' microporous existence (Ahmad and Rahman 2011; Waghmare et al., 2015). According to the Barret-Joyner-Halenda (BJH) method of BET, the pore volumes for RADFP and SMADPFP were 2.2 and 3.1 cm^3/g respectively; they are within the recommendable values mentioned above. The results obtained for BET analysis are also supported by the results obtained manually for pore volume and porosity.

3.1.5. Iodine number

The surface area accessible to tiny adsorbates such as fluoride is measured using the iodine molecule, which is relatively small. The iodine number is used as a measurement for microporosity. The sorption potential increases in direct proportion to the iodine number. Iodine numbers of 150 and 405 mg/g were found in RADFP and SMADFP,

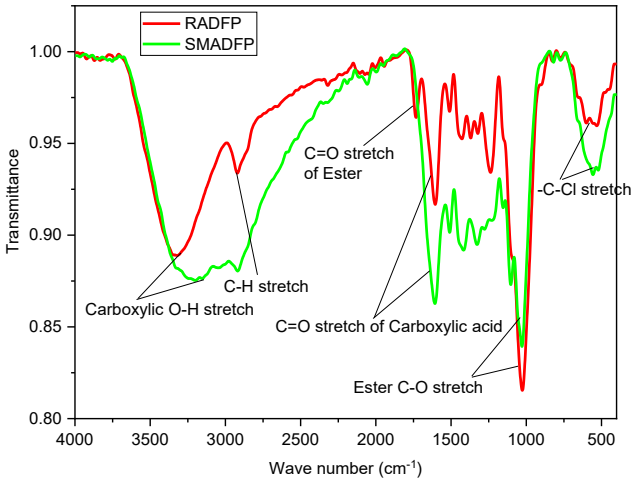

Figure 5. The FT-IR spectra of adsorbents.

respectively. The iodine number of SMADFP is greater than that of RADFP. Devi et al. (2012) portrayed values of 440–700 mg/g, which are much lower in this investigation. This property of RADFP and SMADFP indicates that they have micropores and are capable of removing microscopic particles. The findings from the BET study are in agreement with this finding.

3.1.6. Methylene blue number

The existence of mesopores in a substance can be determined by looking for high values of the methylene blue number. The degree of

Table 2. Establishment of the optimal conditions for nitrate remediation using RADFP, and SMADFP.

Run	pH	Initial Concentration (mg/L)	Contact Time (min)	Adsorbent Dose (g)	Adsorption Efficiency for RADFP (%)	Adsorption Efficiency for SMADFP (%)
1	2.00	27.50	75.00	5.50	64.51	88.95
2	2.00	27.50	30.00	5.50	60.72	88.54
3	2.00	27.50	25.00	5.50	60.12	87.52
4	2.00	5.00	30.00	5.50	61.15	86.15
5	4.00	50.00	120.00	10.00	55.24	82.75
6	6.00	50.00	30.00	10.00	53.15	81.15
7	7.00	5.00	30.00	10.00	50.54	78.20
8	7.00	50.00	25.00	5.50	43.45	76.31
9	7.00	5.00	30.00	1.00	49.15	78.25
10	7.00	27.50	75.00	5.50	52.48	79.65
11	7.00	27.50	75.00	5.50	52.55	79.35
12	7.00	5.00	120.00	10.00	50.12	75.32
13	7.00	50.00	120.00	1.00	50.05	71.95
14	7.00	50.00	25.00	1.00	42.32	72.64
15	7.00	27.50	75.00	5.50	52.87	78.72
16	7.00	27.50	75.00	1.00	46.89	72.86
17	7.00	5.00	120.00	1.00	55.24	69.48
18	12.00	27.50	30.00	5.50	41.17	64.31
19	12.00	27.50	120.00	10.00	42.17	65.12
20	12.00	27.50	75.00	5.50	43.15	68.15
21	12.00	27.50	120.00	5.50	43.51	66.52

mesoporosity of an adsorbent is what determines its ability to adsorb medium-sized molecules, such as the dye methylene blue, in mesopores (Mopoung et al., 2015). RADFP and SMADFP had methylene blue numbers of 120 and 243 mg/g, respectively, indicating the presence of mesopores. The findings of the porosimeter, which suggested that the materials exhibit a feature known as mesoporosity, are supported by this observation, which is compatible with those findings. The results obtained by Bestani et al. (2008) and those obtained by this study for chemically activated plants (130 mg/g) and chemically activated carbon (200 mg/g) are comparable.

3.1.7. Morphology

The morphology of RADFP and SMADFP was visualised by the use of micrographs captured by a scanning electron microscope (SEM) (Fig. 3a and b). These adsorbents feature a porous surface that is randomly dispersed with pores of varying sizes and a surface that is irregularly rough. As a result, these adsorbents have a heterogeneous pore structure. The SEM images demonstrated that the adsorbent's surface had been correctly modified for SMADFP as opposed to RADFP. RADFP has a smoother, fluffier surface than SMADFP, with fewer cracks and voids. Additionally, SEM images showed that SMADFP has a higher porosity and an inner pore structure than RADFP.

3.1.8. Anion exchange capacity

Anion exchange is the mechanism by which ions in solution are moved to a solid matrix, where they are exchanged for ions of a different form but of the same polarity. In other terms, the ions in solutions are replaced by ions from the solid. Because of the adsorbent's exchangeable chloride ions and positively charged adsorbent surface, OH^- adsorption was predominantly based on ion exchange and electrostatic attraction (Hu et al., 2015). In this analysis, the concentration of OH^- ions in the solution were significantly reduced. RADFP and SMADFP had an anion exchange capacity of 3000 and 3360 mg/g, respectively. Both adsorbents are good at adsorbing anions.

3.1.9. pH at point of zero charge

O The pH at the point of zero charge was measured across a range of pH values from 2 to 12, with each point representing an interval of 2 points. The pH_{pzc} value is the pH where the line crosses the axis at pH = 0. Figure 4a and b demonstrates that the adsorbents RADFP and SMADFP were neutral at pH = 5.0 and 7.0, respectively, where $pH_{pzc} = 0$. pH values less than pH_{pzc} suggested that adsorbents had prominences of net positive surface charges and were capable of adsorbing anions (Bakar et al., 2016). As a result, it is predicted that the biosorbents RADFP and SMADFP will eliminate more NO_3^- from aqueous solution at pH values less than 5.0 and 7.0, respectively.

3.1.10. FT-IR analysis

With the use of an FT-IR spectrophotometer, the functional groups of RADFP were examined, as well as the impact of the activation process on the surface functional groups of SMADFP. The wide absorption region between 3500 and 2500 cm^{-1} in the FT-IR spectrum of RADFP is due to carboxylic acid –OH groups that are hydrogen-bonded (spectrum seen in Figure 5 with a red colour). Peaks at 2900 cm^{-1} result from C–H stretching. In the carbonyl range of the spectrum, there are two peaks that can be seen. The presence of carboxylic acid is shown by the peak at 1710 cm^{-1}, whereas the existence of an ester group on the surface of RADFP is indicated by the other peaks at 1740 cm^{-1}. The ester's C–O stretch is responsible for a large peak at 1000 cm^{-1} and multiple weak peaks at 1200 cm^{-1}, providing more evidence for the ester group on the surface. –C–H bending vibrations were found in alkyl halides at 1369–1237.40 cm^{-1}, whereas –C–Cl stretching vibrations were found at 826.16–531.43 cm^{-1} (Pavia et al., 2009).

After the surface of the *Adansonia digitata* fruit pericarp was chemically altered, the peaks of certain functional groups changed, the existence of some functional groups was completely eradicated, and some new functional groups appeared. The peaks between 3500 and 2500 cm^{-1} increase wider as they overlap C–H stretching peaks, which are created by carboxylic acid's O–H stretching vibrations, as shown in the green-colored spectrum in Figure 5. Only one peak in the carbonyl region, at 1710 cm^{-1}, is sharper than RADFP, proving the carboxylic acid group's presence. The SMADFP spectra lost other ester carbonyl peaks, indicating that the ester was changed to carboxylic groups during modification. The presence of alkyl halide –C–Cl stretching was demonstrated by the peak at 826.16–531.43 cm^{-1} (Bakar et al., 2016; Pavia et al., 2009).

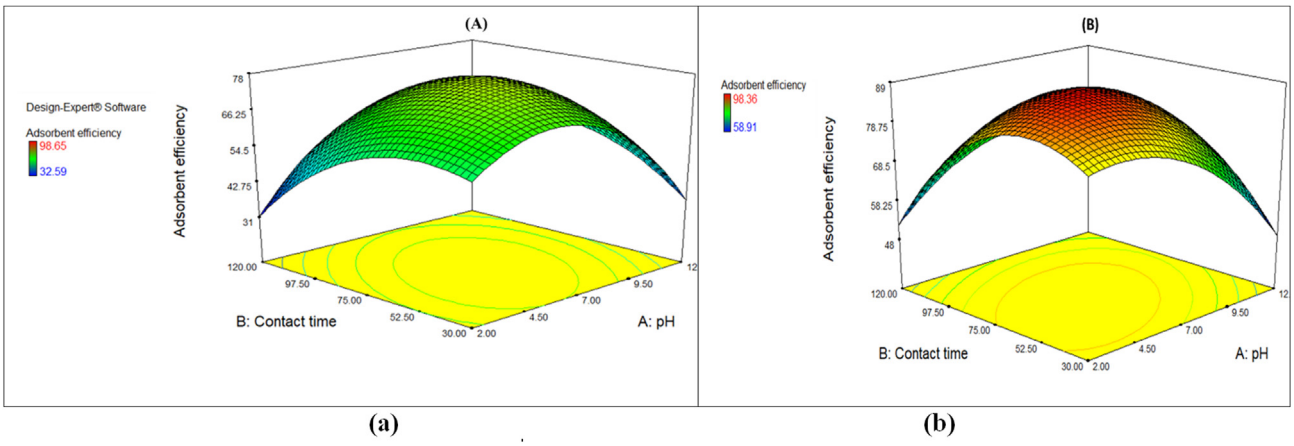

Figure 6. Mutual effect of pH and contact time on the adsorption efficiency of nitrate by **a** RADFP **b** SMADFP.

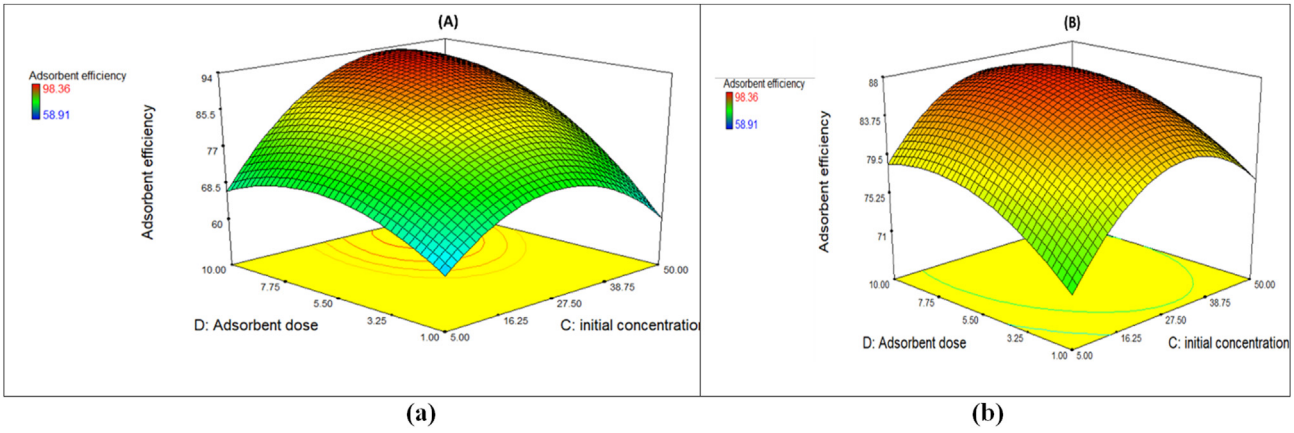

Figure 7. Influence of amount of adsorbent and starting concentration on the adsorption efficiency of nitrate by **a** RADFP, **b** SMADFP.

3.1.11. Establishment of optimal conditions

The RSM offered 21 tests with various operating parameters to find the best operating conditions for maximal pollutant elimination (Table 1). The multiple correlation coefficients, R^2, range between 0.7957 and 0.9950, according to the regression equation produced using analysis of variance (ANOVA). It is important to note that the R^2 value of the model must be 0.75 or higher in order for it to be considered appropriate. According to the findings of the ANOVA, the quadratic model provided a good fit for the experimental data.

The nitrate ion was removed with excellent efficiency by both adsorbents tested. The maximum adsorption efficiencies were determined to be 64.51 and 88.95% for RADFP and SMADFP, respectively, at a pH of 2, a starting concentration of 27.50 mg/L, and an amount of adsorbent of 5.50 g, and interaction period of 75 min (Table 2). It appears that when the pH decreased, the amount of NO_3^- adsorbed increased. The adsorption of NO_3^- ions is accelerated when pH is reduced. In the medium in which the adsorbent is utilized, the interaction between the functional groups and NO_3^- is pH-dependent. In general, nitrate ion remediation increased as pH decreased, which is consistent with Dehghani et al. (2015).

When the pH is high, the amount of time spent in contact with the substance appears to have little impact, which suggests that the adsorption process carried out by biosorbents is pH-dependent. Increasing the contact period from 30 to 75 min at low pH values led to improvements in both the efficiency and capability of adsorption. However, they began to diminish after this period because the available energetic positions and apertures were occupied and saturated with adsorbates. However, increasing the dose of adsorbent increases the number of active sites in the system, which accelerates the adsorption process. Other researchers demonstrated that as the adsorbent dose increased, the number of active sites available for NO_3^- adsorption increased as well. Adsorption efficiency increases with increasing adsorbent dosage. Because intraparticle interactions such as aggregation occur when the adsorbent dose increases, the overall surface area of the adsorbent decreases, the diffusion path length increases, and the adsorption density decreases (Hu et al., 2015). Simultaneously, the initial NO_3^- ion concentration appeared to have a significant impact on adsorption efficiency and capacity. At first, there were a large number of ions vying for available sites and pores, resulting in a high adsorption efficiency and energy. However, both processes began to deteriorate as the majority of the adsorbent's acceptors were exhausted by the adsorbates. This discovery is in line with the findings that were found by Amuda et al. (2014) and Habuda-Stanić et al., 2014.

3.2. Mutual effects of parameters on adsorption efficiency of nitrate

3.2.1. The influence of the pH level and the contact time

Fig. 6a and b illustrate the effect of pH and contact time on the nitrate removal effectiveness of RADFP and SMADFP. At high pH, interaction period had little effect on the adsorption process, but at low pH, it boosted nitrate adsorption efficiency. Thus, a pH of 2 resulted in the extreme elimination of nitrate (64.51 and 88.95%, respectively for RADFP and SMADFP). This is due to the adsorbent's surface being positively charged at low pH. The positively charged surface of the adsorbent and the negatively charged nitrate formed a columbic force of attraction as a result. The adsorbent's surface is significantly protonated in an acidic solution, which draws more nitrate ions to the surface. From this

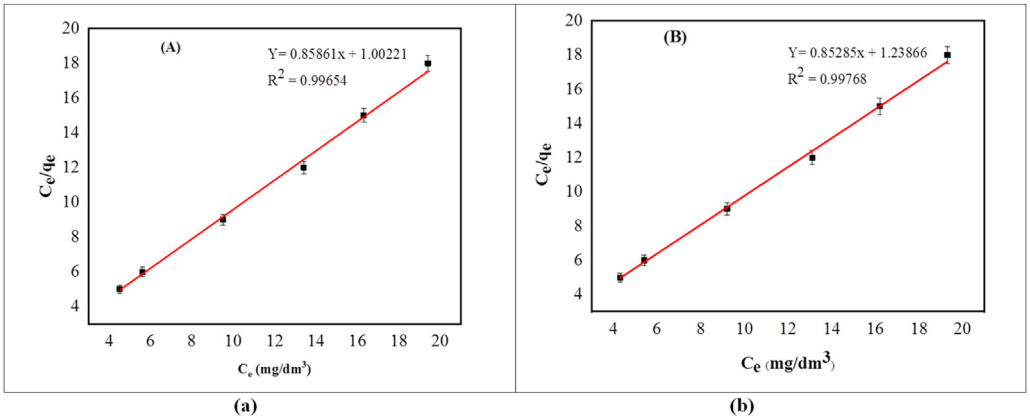

Figure 8. Isotherms of nitrate adsorption using the Langmuir model for remediation by **a** RADFP **b** SMADFP.

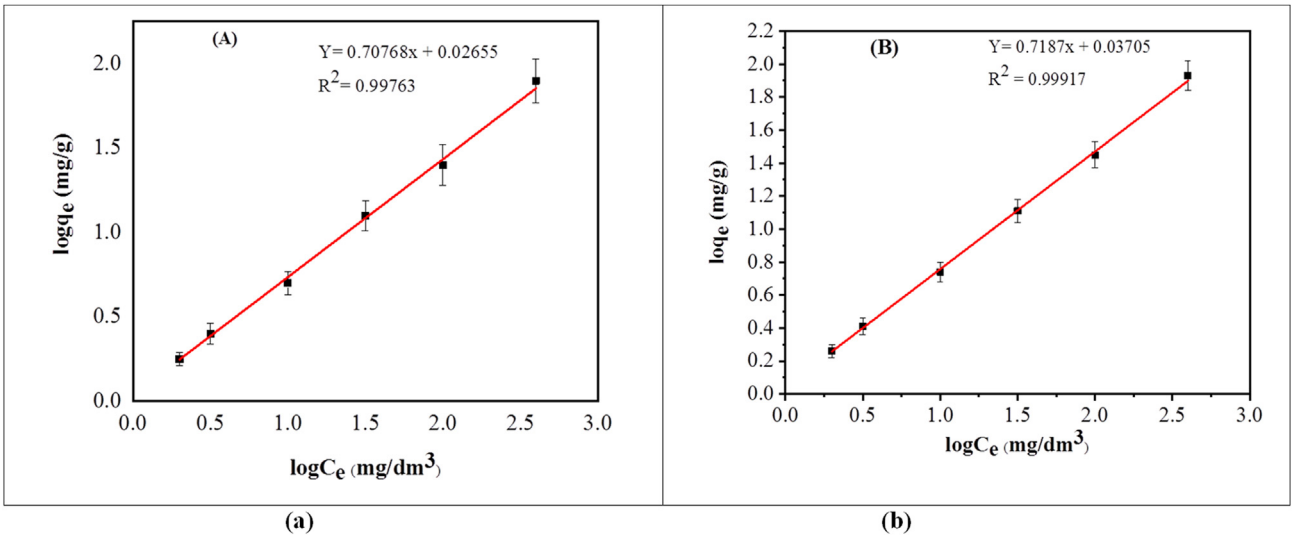

Figure 9. Adsorption isotherms of nitrate according to the Freundlich model by **a** RADFP **b** SMADFP.

experiment, a pH of 2 and interaction period of 75 min are considered the optimal values for achieving the highest adsorption efficiency.

3.2.2. The effect of the amount of adsorbent used and the starting concentration

It's crucial to get this quantity right because the entire adsorption process is dependent on the initial concentration of pollutant ions (Hu et al., 2015). From 5 to 50 mg/L, the impact of the concentration at the start of the experiment was investigated. The outcome of adsorbent dose and starting concentration and its effect on the efficiency of nitrate adsorption is shown in Figures 7a and b. It was demonstrated that the effectiveness of biosorbents in removing nitrate improved as the initial nitrate concentration decreased. This is due to the adsorbent surface using more open energetically active sites capable of attracting the adsorbate. Because all adsorbents have a finite number of active sites, which become saturated at larger concentrations, there is a corresponding decrease in the amount of adsorption that may take place (Namasivayam and Höll 2005; Reddy et al., 2015). The increased adsorbent dose results in a greater number of available nitrate-binding sites. Enhanced availability of nitrate ions per unit mass of adsorbent, i.e., a higher nitrate/adsorbent ratio, is responsible for the increased load capacity. Thus, as shown by the results in Table 1, the adsorption efficiency (%) increased significantly with dosage. Simultaneously, the adsorption potential decreased as the dosage was increased. This is due to the extremely low equilibrium concentration of nitrate, which results in a marginal driving force for adsorption, as well as overlapping of active sites at higher doses and a decline in effective surface area (Masukume et al., 2010). From this experiment, it can be observed that an initial concentration of 27.5 mg/L and an adsorbent dose of 5.50 g is considered optimal values to achieve maximum adsorption efficiency.

3.3. Adsorption isotherms

Experiments of adsorption isotherms were carried out so that the nature of adsorption processes could be determined. In order to provide an accurate representation of the data, the Langmuir and Freundlich adsorption isotherm models were utilised. In order to determine the fundamental characteristics of the adsorption processes, research of adsorption isotherms were carried out. Both the Langmuir and the Freundlich adsorption isotherm models were utilised to analyse the data. The Langmuir adsorption isotherm is described by linearized Eq. (11).

$$\frac{C_e}{q_e} = \frac{C_e}{q_o} + \frac{1}{k_L q_o} \tag{11}$$

Where q_e is the amount of pollutant that is adsorbed per unit weight of adsorbent (mg/g) at equilibrium, C_e is the equilibrium concentration (mg/L), q_o (mg/g) and kL (dm^3/g) are the Langmuir constants, which are

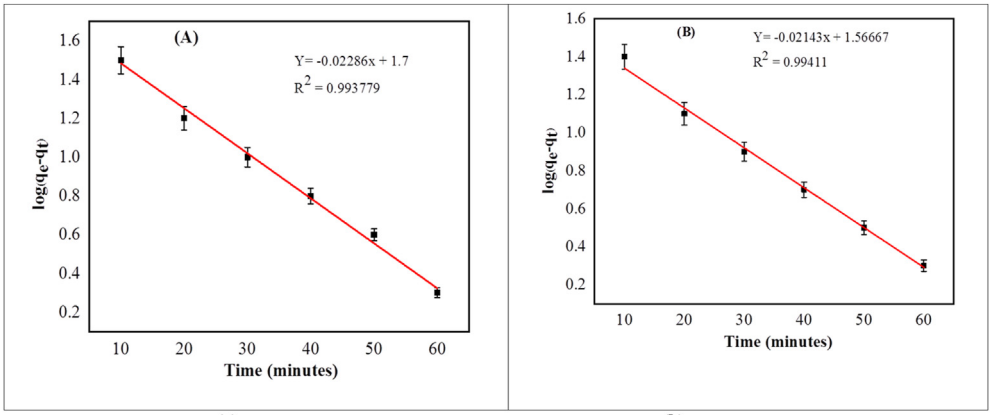

Figure 10. Pseudo-first-order plots for nitrate adsorption by the adsorbents **a** RADFP **b** SMADFP.

related to the adsorption capacity and the energy of adsorption, respectively.

Freundlich isotherm is designated by linearized Eq. (12).

$$\log q_e = \log k_f + \frac{1}{n}\log C_e \quad (12)$$

Where k_f is the Freundlich constant that is measured in L/mg and is related to sorption capacity, and n is the Freundlich exponent that is related to sorption intensity.

3.3.1. Langmuir isotherm

Langmuir isotherm data for nitrate ion adsorption by the adsorbents are indicated in Fig. 8a and b. The Langmuir isotherm was concomitant to the experimental data suggesting favorable adsorption with R^2 values close to 1 for both the adsorbents.

3.3.2. Freundlich isotherm

Figures 9a and b illustrate the Freundlich plots. The linear plots of $\log q_e$ versus $\log C_e$ for both the adsorbents confirm the existence of a Freundlich isotherm concerning the nitrate ions. Freundlich isotherm fitted the adsorption mechanism of nitrate ions by adsorbents well, with correlation coefficient (R^2) values of 0.99763 and 0.99936 respectively for RADFP and SMADFP which are close to 1. The values of n (1.0251 and 1.3989 for raw and modified biosorbents, respectively), a constant called adsorption's intensity lies between 1 and 10 indicating a favorable adsorption process (Ushakumary, 2013).

By varying the isotherm experiments with different adsorbent dosages, both Langmuir and Freundlich's adsorption isotherms were considered. The correlation coefficient can be used to express the power of a linear relationship (R^2). Its value is used to determine the degree to which the isotherm model adequately describes the experimental results. The Langmuir isotherm constants were determined by plotting the specific sorption coefficient (C_e/q_e) against the nitrate-ion equilibrium concentration (C_e), as shown in Fig. 8a and b. The sorption capacities, q_m, are 12.45 and 25.18 mg/g, adsorption coefficient, b, was determined to be 0.0670 and 0.0380, and associated correlation coefficient, R^2, was determined to be 0.99654 and 0.99768 for RADFP and SMADFP respectively for NO_3^- attenuation. Langmuir isotherm's fundamental properties can be expressed in terms of a dimensionless constant separation factor or equilibrium parameter R_L. RADFP and SMADFP have R_L values of 0.1996, and 0.1615, respectively. Since these values are between zero and one, it can be concluded that nitrate adsorption on the adsorbent is favorable under the experimental conditions. The Freundlich parameters and correlation coefficients were determined from experimental data by plotting $\log q_e$ versus $\log C_e$. The Freundlich model is found to have a correlation coefficient of 0.99763 and 0.99917, an adsorption potential of 11.98 and 24.15 mg/g, and adsorption intensity, 1/n, of 0.2100 and 0.3400 respectively for RADFP and SMADFP. Even though the Langmuir model's R^2 values are relatively less than those of the Freundlich model, these values of both the models are very close to 1. Therefore, both the models fitted well to the experimental data.

Table 3. Kinetic parameters obtained from the study of pseudo first-order adsorption.

Adsorbent	k_1 (min^{-1}) (SD, n = 3)	Calculated q_e (mg/g) (SD, n = 3)	Experimental q_e (mg/g) (SD, n = 3)	R^2 (SD, n = 3)
RADFP	0.023 (0.002)	50.119 (1.21)	26.215 (1.34)	0.99378 (0.001)
SMADFP	0.021 (0.001)	36.864 (1.22)	18.573 (1.25)	0.99411 (0.001)

3.4. Kinetics of nitrate adsorption

Experiments based on kinetics were carried out in order to elucidate the process of nitrate adsorption. An investigation into the adsorption process was carried out using pseudo-first-order and pseudo-second-order kinetics. The linearized equation provides a description of the pseudo-first-order model (Eq. 13).

$$\ln(q_e - q_t) = \ln q_e - k_1 t \quad (13)$$

The description of the pseudo-second-order model is represented by Eq. (14).

$$\left(\frac{t}{q_t}\right) = \frac{1}{k_2 q_e^2} + \frac{1}{q_e}(t) \quad (14)$$

Where q_t denotes the nitrate concentration adhered on the adsorbent at any given time (mg of pollutant per g of adsorbent), q_e denotes the amount of nitrate adsorbed per unit weight of adsorbent (mg/g) at equilibrium, k_1 denotes the pseudo-first-order kinetics adsorption rate constant (in min^{-1}), and k_2 is the pseudo-second-order kinetics adsorption rate constant (g/mgmin).

When comparing the mean values of the two kinetic models' linear regression correlation coefficients, R^2 values, the pseudo-second-order model's value (0.98862) is greater than the pseudo-first-order model's value (0.98837). As a consequence, the pseudo-second-order model is the best fit for both adsorbents (Berhe et al., 2015). This means that all steps of adsorption, such as exterior film diffusion, diffusion, and internal particle diffusion, were completed. This model assumes a chemisorption system in which the adsorbent and adsorbate share or transfer electrons. Because it is rate-dependent on the amount of solute adsorbed at any

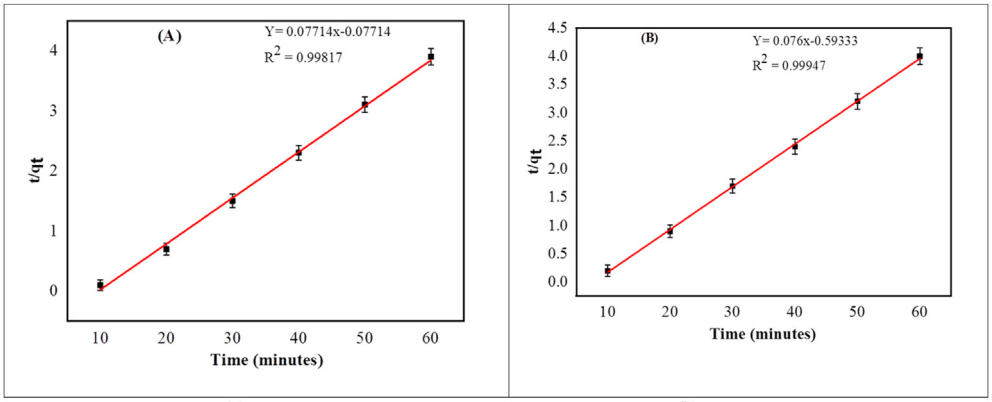

Figure 11. Pseudo-second-order plots for nitrate adsorption by the adsorbents **a** RADFP **b** SMADFP.

Table 4. Kinetic parameters obtained from the study of pseudo second-order adsorption.

Adsorbent	k_2 ($gmg^{-1}min^{-1}$) (SD, n = 3)	Calculated q_e (mg/g) (SD, n = 3)	Experimental q_e (mg/g) (SD, n = 3)	R^2 (SD, n = 3)
RADFP	0.077 (0.01)	12.963 (1.12)	26.215 (1.35)	0.99817 (0.001)
SMADFP	0.076 (0.01)	13.158 (1.54)	12.987 (1.24)	0.99947 (0.0001)

given time, t, and considers adsorption to be the rate-determining step, it occurred under heterogeneous conditions (Echavarria-Alvarez and Hormaza-Anaguano, 2014).

3.4.1. Pseudo-first order

Figures 10a and b show pseudo-first-order plots of (q_e–q_t) against time, t for the adsorption of nitrate by RADFP and SMADFP. k_1 and q_e are calculated using the slope, intercept, and correlation coefficient; R^2 is also determined using the graph. The parameters and graphs indicate that the data do not obey the pseudo-first-order adsorption kinetic model, as the experimental q_e values are not equal to the measured q_e values from the graph (Table 3).

3.4.2. Pseudo-second order

Pseudo-second order kinetic data for the adsorption of nitrate by RADFP and SMADFP are shown in Fig. 11a and b. The slope and intercept were used to get k_2 and q_e, and the graph was used to calculate R^2, the correlation coefficient. The parameters and graphs indicate that the data

Table 5. Comparison of nitrate removal efficiencies by using different adsorbents.

Adsorbent	Removal efficiency (%)	Kinetic study	Adsorption isotherms	Mechanism	Reference
Quarternized biomass	85–92	Pseudo 2nd order	Langmuir and Freundlich	Physisorption, chemisorption, and multilayer sorption.	Namasivayam and Höll (2005).
Modified natural zeolite	80–90	Pseudo 2nd order	Freundlich	Chemisorption and multilayer sorption.	Masukume et al., (2010).
Granular chitosan-Fe^{3+} complex.	95.00	Pseudo 2nd order	Langmuir and Freundlich	Physisorption, chemisorption, and multilayer sorption.	Hu et al., (2015).
Chitin	78.00	Pseudo 2nd order	Langmuir and Freundlich	Physisorption, chemisorption, and multilayer sorption.	Morghi et al., (2015).
New clay	71.89	Pseudo 1st order	Langmuir	Physisorption and monolayer sorption	Ouardi et al., (2015).
Modified steel slag	35.45	Pseudo 2nd order	Freundlich	Chemisorption and multilayer sorption.	Yang et al., (2017).
Local clay	51.00	Pseudo 2nd order	Freundlich	Chemisorption and multilayer sorption.	Battas et al., (2019).
Activated coconut shell charcoal	84.00	Pseudo 2nd order	Freundlich	Chemisorption and multilayer sorption	Sudha et al., (2019).
Activated orange peels	86.00	Pseudo 2nd order	Langmuir and Freundlich	Physisorption, chemisorption, and multilayer sorption	Kumar and Raju (2020).
Thermal activated palm fibers and fronds	72–77	-	Freundlich	Chemisorption and multilayer sorption.	Garamon (2022).
Raw *adansonia digitata* fruit pericarp (RADFP)	64.51	Pseudo 2nd order	Freundlich	Chemisorption and multilayer sorption.	This study
Surface modified *Adansonia digitata* fruit pericarp (SMADFP).	88.95	Pseudo 2nd order	Freundlich	Chemisorption and multilayer sorption.	This study

best fit the pseudo-second-order adsorption kinetic model, as the R^2 value is much closure to unity than that of pseudo-first-order adsorption kinetics and the q_e values from the experiments match the measured q_e from the graph (Table 4).

3.5. Adsorption mechanism

ADFP offers good adsorption properties among other low-cost and easily available materials. It is rich in floral fibre, protein, and a variety of functional groups such as carboxyl, hydroxyl, and amidogen, all of which contribute to its adsorption-promoting properties (Dehghani et al., 2015). The nitrate ion adsorption mechanism is thought to entail an ion exchange process and contact between the adsorbent surface and the NO_3^- (electrostatic attraction or the creation of surface inner-sphere complexes between the anions and hydroxide ions (–OH or $–OH_2^+$)). Furthermore, adsorption into RADFP and SMADFP suggests that acidification has certain advantages in nitrate removal, and that the ion-exchanged process is involved in nitrate binding to the adsorbents.

3.6. Application of adsorbents on the real water

The efficacy of RADFP and SMADFP prepared from *Adansonia digitata* fruit pericarp in removing nitrate was evaluated using real water samples. After treatment with RADFP, the concentrations of nitrate in three groundwater samples were reduced from 55.4, 56.9, and 62.5 mg/L to 46.8, 48.7, and 49.9 mg/L respectively. Even though there is a considerable reduction in the nitrate concentrations, RADFP did not reduce concentrations of NO_3^- to levels below the WHO-allowable limit (45 mg/L for NO_3^-). After treatment with SMADFP, the concentrations of nitrate in three groundwater samples were reduced from 55.4, 56.9, and 62.5 mg/L to 22.4, 25.3, and 27.5 mg/L respectively. The levels of nitrate content in the groundwater samples have been successfully lowered to WHO-acceptable levels for use as drinking water by SMADFP. Based on these findings, it has been concluded that the SMADFP investigated is capable of effectively removing NO_3^- from real water.

3.7. Comparison of the current study with the previous studies

The maximum adsorption efficiency of SMADFP was found to be higher than most natural and modified biosorbents in the literature as shown in Table 2 and Table 5. The isotherm obtained for the sorption of nitrate ions on SMADFP was following what had been previously reported to be a Freundlich isotherm. Most authors in the literature also reported the mechanism of nitrate ions to be via chemisorption and multilayer adsorption except for Ouardi et al. (2015) who reported physisorption and Namasivayam and Höll (2005), Morghi et al. (2015), Hu et al. (2015) and Kumar and Raju (2020) who reported both physisorption and chemisorption.

4. Conclusion

SEM, BET, and IR analysis revealed that the adsorbents exhibited favorable physical and chemical properties for the adsorption of nitrate. BET surface areas of 361.527 and 379.877 m^2/g and pore diameters of 0.3032 and 0.3053 cm^3/g were found for the adsorbents. They had a large proportion of carbonyls, carbon-carbon bonds, and hydroxyl functional groups. As it can be seen in the SEM micrographs, the surface of the adsorbent has a well developed porous structure that is characterised by randomly scattered pores that range in size. Adsorption was significantly influenced by operational variables such as pH, initial nitrate concentration, contact time, and adsorbent dose. In this study, raw (RADFP) and surface-modified (SMADFP) fruit pericarp biosorbents from the *Adansonia digitata* plant were used to remove nitrate from an aqueous solution. The adsorption efficiency improved as the solution's pH and initial concentration of nitrate ions decreased. The rate of nitrate removal increased as the adsorbent dosage was increased, owing to the increased adsorption surface area. The adsorbents prepared from *Adansonia digitata* that are RADFP and SMADFP exhibited the maximum nitrate removal efficiency of 64.55 and 88.95%, respectively, under optimal operating conditions of pH 2, contact time of 75 min, initial concentration of 27.50 mg/L, adsorbent dose of 5.50 g. RADFP and SMADFP have an adsorption capacity, q_0, of 12.45 and 25.18 mg/g, respectively. The adsorption intensity, n, of RADFP and SMADFP is 3.2300 and 5.4500, respectively, which is between 1 and 10, indicating a favorable adsorption phase. The experimental data for the adsorption of nitrate ions fitted well to both Freundlich and Langmuir models with R^2 values of 0.99917 and 0.99763, respectively, and pseudo-second-order kinetic model with R^2 values of 0.99817 and 0.99947, respectively for RADFP and SMADFP. The biosorption experiments performed in this work shed light on the suitability of adsorbents for the attenuation of nitrate. However, It is recommended to perform an economical and availability analysis to see if the sorbent can be applied at a remediation scale.

Declarations

Author contribution statement

David Mihayo, Maheswara Rao Vegi, Said Ali Hamad Vuai: Conceived and designed the experiments; Performed the experiments; Analyzed and interpreted the data; Contributed reagents, materials, analysis tools or data; Wrote the paper.

Funding statement

This research did not receive any specific grant from funding agencies in the public, commercial, or not-for-profit sectors.

Data availability statement

Data included in article/supplementary material/referenced in article.

Declaration of interests statement

The authors declare no conflict of interest.

Additional information

No additional information is available for this paper.

Acknowledgements

The authors would like to express their appreciation to the Department of Chemistry, The University of Dodoma for their constant encouragement during the laboratory work and writing this manuscript.

References

Ahmad, M.A., Rahman, N.K., 2011. Equilibrium, kinetics and thermodynamic of Remazol brilliant orange 3R dye adsorption on coffee husk-based activated carbon. Chem. Eng. J. 170, 154–161.

Al-Fatlawi, A.H., Neamah, M.M., 2015. Batch experiment and adsorption isotherm of phosphate removal by using drinking water treatment sludge and red mud. Int J Adv Res Sci Eng Technol 3 (2), 557–571. https://www.ijarset.com. (Accessed 12 May 2021).

Ali, I., Asim, M., Khan, T.A., 2012. Low-cost adsorbents for the removal of organic pollutants from wastewater. J. Environ. Manag. 113, 170–183.

Amuda, O.S., Olayiwola, A.O., Alade, A.O., Farombi, A.G., Adebisi, S.A., 2014. Adsorption of methylene blue from aqueous solution using steam Activated carbon produced from Lantana camara stem. J. Environ. Protect. 5, 1352–91363.

Assogbadjo, A.E., Chadare, F.J., Manda, L., Sinsin, B., 2021. A 20-Year journey through an orphan African baobab (*Adansonia digitata* L.) towards improved food and nutrition security in Africa. J. Front. Sustain. Food Syst. 5, 675382.

Bakar, A.H.B.A., Koay, Y.S., Ching, Y.C., Abdullah, L.C., Choong, S.Y., Alkhatib, M., Mobarekeh, M.N., Zahri, N.A.M., 2016. Removal of fluoride using quaternized palm kernel shell as adsorbents: equilibrium isotherms and kinetics studies. Bioresources 11 (2), 4485–4511. http://ojs.cnr.ncsu.edu/index.php/BioRes/article. (Accessed 15 May 2021).

Battas, A., Gaidoumi, A.E., Ksakas, A., Kherbeche, A., 2019. Adsorption study for the removal of nitrate from water using local clay. Sci. World J.

Berhe, S., Ayele, D., Tadesse, A., Mulu, A., 2015. Adsorption efficiency of coffee husk for removal of lead (II) from industrial effluents: equilibrium and kinetic Study. Int. J. Sci. Res. Pub. 9 (5), 1–8. https://www.researchgate.net. (Accessed 29 April 2021).

Bestani, B., Benderdouche, N., Benstaali, B., Belhakem, M., Addou, A., 2008. Methylene blue and iodine adsorption onto an activated desert plant. Bioresour. Technol. 99, 8441–8444.

Das, D., Samal1, D.P., Meikap, B.C., 2015. Preparation of activated carbon from green coconut shell and its characterization. J. Chem. Eng. Process Technol. 6, 1–7.

Dehghani, M., Shahsavani, S., Shamsedini, N., Javaheri, M.R., 2015. Removal of nitrate from aqueous solution using rice chaf. Jentashapir J. Health Res. 6 (5), 22–26.

Devi, B.V., Jahagirdar, A.A., Ahmed, M.N.Z., 2012. Adsorption of chromium on activated carbon prepared from coconut shell. Int. J. Eng. Res. Appl. 5 (2), 364–370 https://www.semanticscholar.org. (Accessed 17 May 2021).

Dubey, S.P., Gopal, K., Bersillon, J.L., 2009. Utility of adsorbents in the purification of drinking water: a review of characterization, efficiency and safety evaluation of various adsorbents. J. Environ. Biol. 30 (3), 327–332. https://pubmed.ncbi.nlm.nih.gov. (Accessed 28 May 2021).

Echavarria-Alvarez, A.M., Hormaza-Anaguano, A., 2014. Flower wastes as a low-cost adsorbent for the removal of acid blue 9 Residuos de flores como adsorbentes de bajo costo para la remoción de azul ácido 9. Dyna 81 (185), 132–138.

Elisante, E., Muzuka, A.N.N., 2017. Occurrence of nitrate in Tanzanian groundwater aquifers: a review. Appl. Water Sci. 7, 71–87.

Fan, X., Parker, D.J., Smith, M.D., 2003. Adsorption kinetics of fluoride on low-cost materials. Water Res. 37, 4929–4937.

Garamon, S.E., 2022. Synthesis and characterization of some new non-conventional materials as low-cost adsorbents for removal of nitrates from groundwater in Al-Qurayyat city northern Saudi Arabia. Plant Soil Environ.

Grassi, M., Kaykioglu, G., Belgiorno, V., Lofrano, G., 2012. Removal of emerging contaminants from water and wastewater by adsorption process. In: Lofrano, G. (Ed.), Emerging Compounds Removal from Wastewater. Springer, Dordrecht, pp. 15–37.

Gumus, R.H., Okpeku, I., 2015. Production of activated carbon and characterization from snail shell waste (*Helix pomatia*). Adv. Chem. Eng. Sci. 5, 51–56.

Habuda-Stanić, Mirna, Ravančić, M.E., Flanagan, A., 2014. A review on adsorption of fluoride from aqueous solution. Materials 7, 6317–6366.

Hu, Q., Chen, N., Feng, C., Hu, W., 2015. Nitrate adsorption from aqueous solution using granular chitosan-Fe^{3+} complex. Appl. Surf. Sci. 347, 1–9.

Ideriah, T.J.K., Ikpe, F.N., Nwanjoku, F.N., 2013. Distribution and speciation of heavy metals in crude oil contaminated soils from Niger Delta, Nigeria. World Environ. 3 (1), 18–28.

Jadhav, S.V., Bringas, E., Yadav, G.D., Rathod, V.K., Ortiz, I., Marathe, K.V., 2015. Arsenic and fluoride contaminated groundwaters: a review of current technologies for contaminants removal. J. Environ. Manag. 162, 364–370.

Kihampa, C., 2013. Heavy metal contamination in water and sediment downstream of municipal wastewater treatment plants, Dar es Salaam, Tanzania. Int. J. Environ. Sci. 5 (3), 1407–1415. https://www.researcgate.net. (Accessed 25 April 2021).

Kihampa, C., Mwegoha, W.J.S., 2010. Heavy metals accumulation in vegetables grown along the Msimbazi River in Dar es Salaam, Tanzania. Int. J. Biol. Chem. Sci. 4 (6), 1932–1938.

Kumar, M.V., Raju, H.P., 2020. Nitrate removal from aqueous solution by orange peels as an adsorbent. J. Crit. Rev. 7 (4), 1224–1231.

Masukume, M., Onyango, M.S., Aoyi, O., Otieno, F., 2010. Nitrate removal from groundwater using modified natural zeolite. Chem. Mater. Metall. Eng. 5, 1–13. https://biust.pure.elsevier.com. (Accessed 25 May 2021).

Mihayo, D., Vegi, M.R., Vuai, S.A.H., 2021. Defluoridation of aqueous solution using raw and surface modified biosorbents prepared from *Adansonia digitata* fruit pericarp. J. Dispersion Sci. Technol. 42, 1–13.

Mohsenipour, M., Shahid, S., Ebrahimi, K., 2014. Removal techniques of nitrate from water. Asian J. Chem. 23 (26), 7881–7886.

Mopoung, S., Moonsri, P., Palas, W., Khumpai, S., 2015. Characterization and properties of activated carbon prepared from tamarind seeds by KOH activation for Fe(III) adsorption from aqueous solution. Sci. World J. 2015. Article ID 415961.

Morghi, M., Abidar, F., Soudani, A., Zerbet, M., Chiban, M., Kabli, H., Sinan, F., 2015. Removal of nitrate ions from aqueous solution using chitin as natural adsorbent. Int. J. Res. Environ. Stud. 2, 8–20. www.bluepenjournals.org/ijres. (Accessed 26 April 2021).

Naik, S.S., Setty, Y.P., 2013. Optimization of parameters using response surface methodology and genetic algorithm for biological denitrification of wastewater. Int. J. Environ. Sci. Technol. 11, 823–830.

Namasivayam, C., Holl, W.H., 2005. Quaternized biomass as an anion exchanger for the removal of nitrate and other anions from water. J. Chem. Technol. Biotechnol. 80, 164–168.

National Bureau of Statistics (NBS) [Tanzania], 2017. National Environment Statistics Report, 2017 (NERS, 2017), Dar Es Salaam Tanzania Mainland.

Ogata, F., Nagai, N., Kariya, Y., Nagahashi, E., Kobayashi, Y., Nakamura, T., Kawasaki, N., 2018. Adsorption of nitrite and nitrate ions from an aqueous solution by Fe–Mg-type hydrotalcites at different molar ratios. Chem. Pharm. Bull. 66, 458–465.

Ouardi, M.E., Qourzal, S., Alahiane, S., Assabbane, A., Douch, J., 2015. Effective removal of nitrate ions from aqueous solution using new clay as potential low-cost adsorbent. J. Encapsulation Adsorpt. Sci. 5, 178–190.

Pavia, D.L., Lapman, G.M., Kriz, G.S., Vyvyan, J.R., 2009. Introduction to Spectroscopy, fourth ed. Brooks/Cole, Cengage Learning, Bellingham, Washington, pp. 25–104.

Rangari, P.J., Chavan, P., 2017. Preparation of activated carbon from coconut shell. Int. J. Innov. Res. Sci. Eng. Technol. 7 (6), 220–225. https://www.ijirset.com. (Accessed 17 May 2021).

Reddy, C.A., Prashanthi, N., Babu, P.H., Mahale, J.S., 2015. Banana peel as a biosorbent in removal of nitrate from water. Int. Adv. Res. J. Sci. Eng. Technol. 10 (2), 94–98.

Soumya, G.N., Manickavasagam, M., Santhanam, P., Kumar, S.D., Prabhavathi, P., 2015. Removal of phosphate and nitrate from aqueous solution using seagrass *Cymodocea rotundata* beads. Afr. J. Biotechnol. 14 (16), 1393–1400.

Sudha, N., Priyadharshini, P., Subaranjani, J.S., Pradeepa, K., 2019. Removal of nitrate from water by using activated coconut shell charcoal. Inter. J. Adv. Res. Innov. 4, 1–4.

Sumiya, U., Anu, N., 2016. Nitrate removal from synthetic wastewater by using bio-adsorbent. Int. J. Eng. Res. 4 (7), 307–309. https://www.ijser.org. (Accessed 17 May 2021).

Tan, I.A.W., Ahmad, A.L., Hameed, B.H., 2008. Preparation of activated carbon from coconut husk: optimization study on removal of 2,4,6-trichlorophenol using response surface methodology. J. Hazard Mater. 153, 709–717.

Tan, X., Liu, Y., Zeng, G., Wang, X., Hu, X., Gu, Y., Yang, Z., 2015. Application of biochar for the removal of pollutants from aqueous solutions. Chemosphere 125, 70–85.

Tarachand, N., Dipak, S., 2016. Baobab fruit shell (*Adansonia digitata*) as a natural adsorbent for copper and lead removal from industrial effluent. Res. J. Chem. Environ. Sci. l 4 (2), 32–38. https://www.aelsindia.com/rjces.htm. (Accessed 29 May 2021).

Tukur, R., Rabi'u, M., 2013. An assessment of multi-purpose use of *Adansonia digitata* (baobab tree) for sustainable development in the semi urban fringes of Dutsinma Katsina State Nigeria. Acad. Res. Int. 1 (4), 486–494. www.journals.savap.org.pk. (Accessed 23 April 2021).

Ushakumary, E.R., 2013. Waste Water Treatment Using Low-Cost Natural Adsorbents. Dissertation, Cochin University of Science and Technology, Kerala, India.

Verla, A.W., Horsfall1, M., Verla, E.N., Spiff1, A.I., Ekpete, O.A., 2012. Preparation and characterization of activated carbon from fluted pumpkin (*Telfairia occidentalis* hook.F) seed shell. Asian J. Nat. Appl. Sci. 3 (1), 39–50. https://www.scirp.org. (Accessed 19 May 2021).

Waghmare, S., Arfin, T., Rayalu, S., Lataye, D., Dubey, S., Tiwari, S., 2015. Adsorption behaviour of modified zeolite as novel adsorbents for fluoride removal from drinking water: surface phenomena, kinetics and thermodynamics studies. Int. J. Sci. Eng. Technol. Res. 12 (4), 4114–4124. https://www.semanticscholar.org. (Accessed 4 May 2021).

WHO, 2011. Nitrate and Nitrite in Drinking-Water: Background Document for Development of WHO Guidelines for Drinking-Water Quality. www.who.int/about/licensing/copyright_form/en/index. Html. (Accessed 16 April 2021).

Yang, L., Yang, M., Xu, P., Zhao, X., Bai, H., Li, H., 2017. Characteristics of nitrate removal from aqueous solution by modified steel slag. Water 757 (9), 1–17.

Zhang, Z.G., Cao, S.G., Li, Y., Guo, P., Yang, H., Yang, T., 2018. Effect of moisture content on methane adsorption and desorption-induced deformation of tectonically deformed coal. Adsorpt. Sci. Technol. 36 (9–10), 1648–1668.

Zhu, P., Wang, H., Sun, B., Deng, P., Hou, S., Yu, Y., 2009. Adsorption of fluoride from aqueous solution by magnesia-amended silicon dioxide granules. J. Chem. Technol. Biotechnol. 84, 1449–1455.